

SUPER-TWISTING CONTROL WITH QUATERNION FEEDBACK FOR LINE-OF-SIGHT STABILIZATION AND TRACKING

MATHEUS F. REIS, RAMON R. COSTA*, ANTONIO C. LEITE†

*COPPE/UFRJ

Ilha do Fundão, Rio de Janeiro, RJ, Brasil

†PUC-Rio

Gávea, Rio de Janeiro, RJ, Brasil

matheus.ferreira.reis@gmail.com, ramon@coep.ufrj.br, antonio@ele.puc-rio.br

Abstract— The majority of works in line of sight (LOS) stabilization and tracking using inertially stabilized platforms (ISP) apply simple linear controllers to achieve the required performance. Commonly, linear models such as a double integrator with an inertia gain are employed to describe the relationship between torque and position of the ISP joints. However, these techniques do not provide ideal disturbance rejection or finite-time convergence, which are desired characteristics for these type of systems in the context of high-accuracy applications. In this work, we propose a Sliding Mode Control (SMC) strategy for both stabilization and orientation tracking for a 3-DOF ISP. Full state feedback and output feedback cases are considered. In the latter case, a High-Order Sliding Mode observer (HOSMO) is proposed for the estimation of the ISP joint velocities. In each case, two Super Twisting Controllers (STC) are employed in a cascade topology. The inner controller ideally rejects the *dynamic* disturbances acting on the ISP joints, reducing the system to an ideal double integrator. The outer controller ensures orientation tracking in quaternion space, ideally rejecting all remaining kinematic disturbances. Numerical simulations show the efficiency and performance of the proposed controller and observer.

Keywords— line-of-sight stabilization, inertial platforms, super-twisting control, higher-order sliding modes observers

1 Introduction

Line-of-sight (LOS) stabilization is a challenging problem. Inertially stabilized platforms (ISP) are widely used for payload stabilization and tracking applications, when a sensor must accurately point to a target in a dynamic environment. Some examples are cameras for aerial surveying and entertainment industry (Hurák and Rezáč, 2009), long-range sensors on vehicles (Debruin, 2008), military applications (Kazemy et al., 2007) and thermal cameras for oil spill detection (Skjelten et al., 2011).

ISPs are motor-driven, gimballed structures, usually mounted on a vehicle with a payload fixed on its last gimbal. Gyroscopes or inertial navigation systems (INS) are employed in the control loop by either measuring the vehicle motion (*indirect stabilization*) or directly measuring the payload motion (*direct stabilization*) (Kennedy and Kennedy, 2003). The latter is usually recommended for precision pointing applications, since the sensor location is appropriate for capturing other effects that can impact the measured angular rates, such as structure flexibility, resolvers, tachometer and/or encoder accuracy and processor sampling rate (Kennedy and Kennedy, 2003). A possible drawback of this method is the larger size of the gimbals required to support the larger payload induced by the weight of the sensors in the inner gimbal. This drawback is usually absent in the indirect method.

The typical control topology usually found in literature is P-PI control. Usually, the inner PI ve-

locity loop has a high bandwidth to stabilize the payload and attenuate the torque disturbances. The outer proportional orientation loop operates at a lower bandwidth and minimizes the pointing error (Hilkert, 2008), (Masten, 2008), (Kennedy and Kennedy, 2014). However, in *high accuracy* and/or *fast dynamics* applications, unmodeled effects may add significant torque contributions, and simple linear controllers may not suffice for the required level of performance.

Some works have tackled the problem of LOS control for ISPs in a more detailed way. In (Abdo et al., 2013), the effects of kinematic coupling of the base and gimbal imbalance are analyzed for a 2-DOF ISP, while (Abdo et al., 2014) proposes a self-tuning PID-type fuzzy controller as an alternative to PID control used in the ISP internal stabilization loop. Recently, (Königseder et al., 2017) used the unit quaternion formalism for attitude stabilization, proposing a control method based in feedback linearization that takes partial advantage of the ISP Lagrangian model. In (Reis et al., 2018), it is shown that even in the presence of large parameter uncertainties, a computed-torque plus PID (CTPID) controller guarantees satisfactory performance.

Modern techniques using Sliding Mode Control (SMC) are being applied for ISP stabilization and tracking. Their attractive characteristics include: (i) exact rejection of bounded matched disturbances; (ii) finite-time convergence and (iii) ease of implementation. For example, in (Mao et al., 2017), a Non-singular Terminal Sliding Mode controller (Feng et al., 2002) is used to achieve finite-time stabilization of an ISP in the

presence of bounded matched disturbances affecting its electromechanical system. To avoid measuring the system state, High-Order Sliding Mode (HOSM) observers are employed (Levant, 2003).

In this work, a cascade control strategy based on the super-twisting algorithm (STA) is used to tackle the problem of ISP stabilization and tracking. Two cases are considered: (i) full state feedback, where the ISP joint angles and velocities are measured and (ii) output feedback, where the ISP joint velocities are estimated using an observer based on higher-order sliding mode (HOSM) theory. Stability analysis is performed, and numerical simulations show the efficiency and performance of the proposed control schemes.

2 ISP Modeling

In this section, a procedure for deriving the kinematic and dynamic models of an ISP installed on a moving base is presented. Let body 0 be the moving base and bodies 1, 2, 3 be the ISP gimballs. Also, if a superscript is omitted, the vector is written in world frame \mathbf{E}_w coordinates.

2.1 Quaternion-Based Kinematics

Let $R \in SO(3)$ be a *rotation matrix* describing the rotation from an arbitrary frame to another. Then, R is a diffeomorphism with respect to the projective space $\mathbb{RP}^3 = \{\|v\|^2 \leq \pi \mid v \in \mathbb{R}^3\}$. Therefore, each point $v \in \mathbb{RP}^3$ is a 4-parameter representation for $SO(3)$ called the *angle-axis*, where the unitary vector on the direction of v represents the rotation axis and $\|v\|$ represents the corresponding rotation angle around that axis.

Remark 1 Note that \mathbb{RP}^3 covers $SO(3)$ twice, since any point on it actually represents the same rotation than the opposite point of the sphere.

This representation can be expressed by $v = \{\theta, n\}$, where $\theta \in \mathbb{R}$ is the angle of rotation around the unit axis vector $n \in \mathbb{R}^3, \|n\| = 1$. Another non-minimal representation is the *unit quaternion*. The set of *quaternions* \mathbb{H} is:

$$\mathbb{H} := \{\eta + i\epsilon_1 + j\epsilon_2 + k\epsilon_3 \mid \eta, \epsilon_1, \epsilon_2, \epsilon_3 \in \mathbb{R}\},$$

$$i^2 = j^2 = k^2 = ijk = -1. \quad (1)$$

A quaternion $Q \in \mathbb{H}$ can also be represented as the pair $Q := \{\eta, \epsilon\}$, where $\eta = \text{Re}(Q) \in \mathbb{R}$ represents the *real* part of the quaternion and $\epsilon = \text{Im}(Q) = [\epsilon_1 \ \epsilon_2 \ \epsilon_3]^\top \in \mathbb{R}^3$ represents the vector part. The quaternion *conjugate* is given by $Q^* = \{\eta, -\epsilon\}$. One can also represent the quaternion in fully vector form by the notation $\bar{Q} = [\eta \ \epsilon_1 \ \epsilon_2 \ \epsilon_3]^\top \in \mathbb{R}^4$.

Quaternions also form an algebraic *group* with respect to *multiplication*. Given two quaternions $Q_1 = \{\eta_1, \epsilon_1\}$ and $Q_2 = \{\eta_2, \epsilon_2\}$, their multiplication follows the rules established by (1):

$$Q_1 \circ Q_2 = \{\eta_1\eta_2 - \epsilon_1^\top \epsilon_2, \eta_1\epsilon_2 + \eta_2\epsilon_1 + \epsilon_1 \times \epsilon_2\}. \quad (2)$$

Quaternion multiplication can also be performed as a linear transformation in \mathbb{R}^4 , by:

$$\overline{Q_1 \circ Q_2} = \mathbf{H}_+(Q_1) \bar{Q}_2, \quad (3)$$

$$= \mathbf{H}_-(Q_2) \bar{Q}_1, \quad (4)$$

where \mathbf{H}_+ , \mathbf{H}_- are *Hamilton operators* defined by

$$\mathbf{H}_\pm(Q) = [\bar{Q} \ \mathbf{h}_\pm(Q)], \quad \mathbf{h}_\pm(Q) = \begin{bmatrix} -\epsilon^\top \\ \eta \mathbf{I}_3 \pm \hat{\epsilon} \end{bmatrix} \quad (5)$$

The square of the quaternion *norm* is defined as the *scalar*

$$\|Q\|^2 = Q \circ Q^* = \{\eta^2 + \epsilon^\top \epsilon, 0\}, \quad (6)$$

and its *inverse* is the quaternion Q^{-1} such that $Q \circ Q^{-1} = \mathbf{I}_Q = \{1, 0\}$, the *unitary* quaternion.

The set of *unit quaternions* $\mathbb{H}^* = \{Q \in \mathbb{R} : \|Q\| = 1\}$ can be used as a parametrization for orientation in the following way. For an element $p = \{\theta, n\} \in \mathbb{RP}$, define:

$$Q = \left\{ \cos\left(\frac{\theta}{2}\right), \sin\left(\frac{\theta}{2}\right) n \right\} \in \mathbb{H}^*. \quad (7)$$

Remark 2 The inverse of an unit quaternion is given by $Q^{-1} = Q^*$, which according to (7), corresponds to the opposite rotation due to negative direction of the rotation axis n .

Let $r_0, r_1, \dots, r_n \in \mathbb{H}^*$ be the n absolute rotations between frames $\mathbf{E}_0, \mathbf{E}_1, \dots, \mathbf{E}_n$ and the world frame \mathbf{E}_w , and $r_{i+1}^i \in \mathbb{H}^*$ ($i = 1, 2, \dots, n-1$) represent the rotations from frame \mathbf{E}_i to \mathbf{E}_{i+1} . Since the unit quaternions form a group with respect to multiplication, then

$$r_n = r_1 \circ r_2^1 \circ \dots \circ r_n^{n-1} \in \mathbb{H}^*. \quad (8)$$

Now, define the set of *pure quaternions* $\mathbb{H}_p = \{v \in \mathbb{H} : \text{Re}(v) = 0\}$. Note that any vector from \mathbb{R}^3 can be represented as the vector part of a corresponding element $v \in \mathbb{H}_p$. Let v^i and $v^j \in \mathbb{H}_p$ be representations for a vector \vec{v} in frames \mathbf{E}_i and \mathbf{E}_j , respectively, and r_j^i represents the rotation from \mathbf{E}_i to \mathbf{E}_j , with unitary axis $n_j^i \in \mathbb{R}^3$ and rotation angle θ_{ij} . Then, the following relation holds:

$$v^i = (r_j^i) \circ v^j \circ (r_j^i)^* = Ad_{r_j^i} [v^j], \quad (9)$$

where $Ad_{r_j^i}[*]$ is the *adjoint operator*. Note that, in vector algebra, $Ad_{r_j^i}$ represents the corresponding rotation matrix $R_{ij} \in SO(3)$ associated to the

unit quaternion $r_j^i \in \mathbb{H}^*$. In terms of the components of r_j^i , this matrix is given by

$$R_{ij} = N_j^i + s_{ij} \mathbf{S}(n_j^i) + c_{ij} (\mathbf{I}_3 - N_j^i) \quad (10)$$

where $N_j^i = n_j^i (n_j^i)^\top$ and s_{ij} and c_{ij} are the sine and cosine functions of θ_{ij} . The rotation matrix corresponding to an absolute rotation $r_i \in \mathbb{H}^*$ is written with only one subscript, as $R_i \in SO(3)$.

Now, let \vec{v}_i and $\vec{\omega}_i$ be the physical linear and angular velocities of \mathbf{E}_i . They are represented by $v_i^i \in \mathbb{R}^3$ and $\omega_i^i \in \mathbb{R}^3$ when written in its own body frame. Let $r_i = \{\eta_i, \epsilon_i\} \in \mathbb{H}^*$ be the absolute rotation of \mathbf{E}_i . The time-derivative of r_i can be related to ω_i^i by

$$\dot{r}_i = \begin{bmatrix} \dot{\eta}_i \\ \dot{\epsilon}_i \end{bmatrix} = \frac{1}{2} \mathbf{h}_+(r_i) \omega_i^i, \quad (11)$$

which is known as the *quaternion propagation* formula (Vilhena Adorno, 2017).

The vector $V_i^i = [(v_i^i)^\top (\omega_i^i)^\top]^\top \in \mathbb{R}^6$ is the *body velocity twist* associated to \mathbf{E}_i . Two body velocity twists associated to different frames $\mathbf{E}_i, \mathbf{E}_j$ located in the *same rigid-body* are related through the constant adjoint map $Ad_{g_{ij}} \in \mathbb{R}^{6 \times 6}$:

$$V_i^i = Ad_{g_{ij}} V_j^j, \quad Ad_{g_{ij}} = \begin{bmatrix} R_{ij} & \mathbf{S}(p_{ij}^i) R_{ij} \\ 0 & R_{ij} \end{bmatrix}, \quad (12)$$

where $\mathbf{S}(\ast) \in so(3)$ is the cross-product operator.

Now, recall that ω_i^i can be written as the sum $\omega_i^i = \omega_0^i + \omega_{0,i}^i$ and can be expressed in terms of $q, \dot{q} \in \mathbb{R}^3$ by means of the *angular body link Jacobian* $J_{0i}^i(q, \Pi_g) \in \mathbb{R}^{3 \times 3}$ as $\omega_{0,i}^i = J_{0i}^i(q, \Pi_g) \dot{q}$:

$$\omega_i^i = J_{0i}^i(q, \Pi_g) \dot{q} + \omega_0^i, \quad (13)$$

where Π_g is the vector of *geometric* parameters of the ISP, containing combinations of components of the axes and distance vectors of each link frame. Note that the body link Jacobian $J_{0i}^i(q, \Pi_g)$ can be computed numerically using iterative algorithms.

These kinematic relations can be used to describe the dependence among vehicle, ISP and camera motion by applying the group operation of \mathbb{H}^* , equation (13) and its time-derivative, with the camera frame \mathbf{E}_c , yielding

$$r_c = r_0 \circ r_c^0(q, \Pi_g), \quad (14)$$

$$\omega_c^c = J_{0c}^c(q, \Pi_g) \dot{q} + \omega_0^c, \quad (15)$$

$$\dot{\omega}_c^c = J_{0c}^c(q, \Pi_g) \ddot{q} + \dot{J}_{0c}^c(q, \dot{q}, \Pi_g) \dot{q} + \dot{\omega}_0^c. \quad (16)$$

An important algebraic property is the *linearity* of (15) with respect to the *geometric* parameters (Siciliano et al., 2009):

$$\omega_c^c = W_\omega(q, \dot{q}, \omega_0^c) \Pi_g. \quad (17)$$

where $W_\omega \in \mathbb{R}^{3 \times N_g}$ is a *kinematic regressor*.

2.2 Dynamic Equations

In (From et al., 2014), it is shown that the equations of motion for a vehicle-manipulator system (VMS) with respect to the vehicle frame \mathbf{E}_0 can be written as:

$$M_{qq} \ddot{q} + C_{qq} \dot{q} + G_q + M_{qV} \dot{V}_0^0 + C_{qV} V_0^0 = \tau_q, \quad (18)$$

where $\tau_q \in \mathbb{R}^n$ is the vector of generalized forces acting on the robot joints, collocated with \dot{q} . Matrices $M_{qq}(q, \Pi_g, \Pi_d) \in \mathbb{R}^{3 \times 3}$ and $M_{qV}(q, \Pi_g, \Pi_d) \in \mathbb{R}^{3 \times 6}$ are mass matrices, $C_{qq}(q, \dot{q}, V_0^0, \Pi_g, \Pi_d) \in \mathbb{R}^{3 \times 3}$ and $C_{qV}(q, \dot{q}, V_0^0, \Pi_g, \Pi_d) \in \mathbb{R}^{3 \times 6}$ are Coriolis matrices and $G_q(q, r_0, \Pi_g, \Pi_d) \in \mathbb{R}^3$ is the gravity vector. Since an ISP composed of rigid links installed on a moving base is a VMS, its dynamic model is identical to (18).

It is worth mentioning that, in a similar way than in (17), (18) is also *linear* with respect to the *dynamic* parameters (Siciliano et al., 2009):

$$Y_q(q, \dot{q}, \ddot{q}, r_0, V_0^0, \dot{V}_0^0, g, \Pi_g) \Pi_d = \tau_q, \quad (19)$$

where $Y_q \in \mathbb{R}^{3 \times N_d}$ is a *dynamic regressor*.

It is worth mentioning that the ISP dynamics (18) and some of its individual terms can be computed iteratively by means of a computationally efficient algorithm known as the *Newton Euler* method (Siciliano et al., 2009).

3 Problem Formulation

Consider a ISP on a moving base (vehicle) with dynamics given by (18), rewritten here as:

$$M_{qq} \ddot{q} + \tau_d = u, \quad (20)$$

where $u(t) = \tau_q$ is the control signal and $\tau_d = C_{qq} \dot{q} + G_q + M_{qV} \dot{V}_{0b}^b + C_{qV} V_{0b}^b$ is a nonlinear disturbance. Given an orientation reference $r_{c_d}(t) \in \mathbb{H}^*$ and an angular velocity reference $\omega_{c_d}^c(t) \in \mathbb{R}^3$ for the camera, the *control objective* is to find a control law $u(t)$ that ensures that the camera quaternion and angular velocity errors

$$e_c = r_c^* \circ r_{c_d}(t), \quad (21)$$

$$e_\omega = \omega_{c_d}^c(t) - \omega_c^c, \quad (22)$$

converge to their respective zero elements \mathbf{I}_Q and 0 , respectively, despite of the system disturbances. Note that when $r_c = r_{c_d}(t)$, the orientation error (21) is the unit quaternion \mathbf{I}_Q .

The desired camera orientation is

$$R_{c_d} = [x_{c_d} \ y_{c_d} \ z_{c_d}] \in SO(3). \quad (23)$$

Let \mathbf{E}_t be the target frame with *given* position p_t , velocity \dot{p}_t , and acceleration \ddot{p}_t . Define

$$p_{ct} = p_t - p_c = [x_{ct} \ y_{ct} \ z_{ct}]^\top,$$

where $p_c \in \mathbb{R}^3$ is the camera inertial position. Some conditions must be applied to find the expression for R_{c_d} that ensures the correct LOS. They can be expressed in terms of two constraints:

- (i) $x_{c_d} = \frac{p_{ct}}{\|p_{ct}\|}$ (pointing condition),
- (ii) $y_{c_d} = \frac{z_0 \times p_{ct}}{\|z_0 \times p_{ct}\|}$ (zero roll condition).

With these two constraints, the last column of R_{c_d} can be computed simply as $z_{c_d} = x_{c_d} \times y_{c_d}$. Then, the mapping from $R_{c_d} \in SO(3)$ to $r_{c_d} \in \mathbb{H}^*$ is relatively straightforward and can be found in (Siciliano et al., 2009), for example.

For mobile target tracking, the angular velocity and acceleration references for the camera are

$$S(\omega_{c_d}^c) = R_{c_d}^T \dot{R}_{c_d}, \quad (24)$$

$$S(\dot{\omega}_{c_d}^c) = \dot{R}_{c_d}^T \dot{R}_{c_d} + R_{c_d}^T \ddot{R}_{c_d}, \quad (25)$$

where \dot{R}_{c_d} , \ddot{R}_{c_d} can be computed from the time derivatives of x_{c_d} , y_{c_d} , and z_{c_d} , which are dependent on \dot{p}_{ct} and \ddot{p}_{ct} .

Remark 3 In fact, $\omega_{c_d}^c \in \mathbb{R}^3$ is linear with respect to $\dot{p}_{ct} \in \mathbb{R}^3$:

$$\omega_{c_d}^c = Z(p_{ct}) \dot{p}_{ct}, \quad Z(p_{ct}) \in \mathbb{R}^{3 \times 3}. \quad (26)$$

4 Super-Twisting Control with Quaternion Feedback

In this section, a second-order sliding mode (SOSM) controller based on super-twisting algorithm (STA) will be developed for the stabilization and tracking of the ISP. Two cases are considered: super-twisting control (STC) with full state feedback and with output feedback only.

The dynamic model (20) can be rewritten as

$$\begin{aligned} \dot{x}_1 &= x_2, \\ \dot{x}_2 &= M_{qq}^{-1}(x_1, \Pi) \tau_q + x_3(x_1, x_2, \Pi, t), \end{aligned} \quad (27)$$

where the states $x_1 = q$, $x_2 = \dot{q}$ are the ISP joint angles and velocities and $x_3 = -M_{qq}^{-1}(x_1) \tau_d$ is a state-dependent disturbance.

Remark 4 Note that, under assumption of torque control $u(t) = \tau_q$, state-space model (27) is a double-integrator with a nonlinear high-frequency gain and a matched disturbance x_3 .

Now, in a similar way than in (27), (11) and (16) can be rewritten as

$$\begin{aligned} \dot{y}_1 &= 0.5 \mathbf{h}_+(y_1) y_2, \\ \dot{y}_2 &= J_{0c}^c(x_1, \Pi_g) \dot{x}_2 + y_3(x_1, x_2, \Pi_g, t). \end{aligned} \quad (28)$$

where the state $y_1^T = \bar{r}_c^T = [y_{11} \ y_{12}^T]$ is the vector representation of the camera orientation $r_c \in \mathbb{H}^*$,

with $y_{11} = \eta_c$ and $y_{12} = \epsilon_c$ being the scalar and vector components. State $y_2 = \omega_c^c$ is the camera body angular velocity, while $y_3 = \dot{J}_{0c}^c \dot{q} + \dot{\omega}_0^c$ is another state-dependent disturbance. Given the references $r_{c_d}(t) \in \mathbb{H}^*$ and $\omega_{c_d}^c(t) \in \mathbb{R}^3$ for the camera, $\bar{r}_{c_d}^T(t) = y_{1d}^T(t) = [y_{11d}(t) \ y_{12d}^T(t)]$ and $\omega_{c_d}^c(t) = y_{2d}(t)$.

Remark 5 Note that the state-space model (28) is a double integrator with a nonlinear high-frequency gain and a matched disturbance y_3 with respect to a control input \dot{x}_2 .

This structure strongly suggests the use of a cascade controller for both stabilization and tracking. An inner controller acts on $u(t)$ in (27) to control \dot{x}_2 , providing dynamic stabilization for the system, while an outer tracking controller acts on \dot{x}_2 in (28), controlling the camera orientation y_1 .

4.1 Super-Twisting Control with Full State Feedback

Suppose that both ISP states x_1 and x_2 are available. The following theorem provides an stability analysis for the proposed sliding mode cascade controller.

Theorem 1 (Cascade STC with Full State Feedback)

Let (27) and (28) be the system dynamic and kinematic models. Assume the following:

- (i) the body Jacobian $J_{0c}^c \in \mathbb{R}^{3 \times 3}$ is full-rank;
- (ii) \dot{q} and \ddot{q} are uniformly norm-bounded;
- (iii) V_0^0 , \dot{V}_0^0 and \ddot{V}_0^0 are uniformly norm-bounded.

Define the super-twisting control expression

$$S_t(s, A, B) = A |s|^{1/2} + B \int_0^t \text{sgn}(s) d\tau,$$

with $A, B > 0$ and operator $|s|^\alpha: \mathbb{R}^n \rightarrow \mathbb{R}^n$, with its elements given by $\|s_i\|^\alpha \text{sgn}(s_i)$, where $s_i \in \mathbb{R}$ is the i -th element of $s \in \mathbb{R}^n$ and $\alpha \in \mathbb{R}$.

The outer sliding surface is

$$s_y = e_\omega + K_c \text{Im}(e_c), \quad K_c > 0, \quad (29)$$

where $K_c > 0$. The outer control law $w(t) \in \mathbb{R}^3$ is implicitly given by

$$\hat{J}_{0c}^c w(t) = \dot{y}_{2d} + K_c \psi + S_t(s_y, \Lambda_3, \Lambda_4), \quad (30)$$

where $\hat{J}_{0c}^c = J_{0c}^c(x_1, \hat{\Pi}_g)$ and ψ is a function of y_1 , y_2 and r_{c_d} . The inner sliding surface is defined as

$$s_x = x_2 - \int_0^t w(\tau) d\tau, \quad (31)$$

and the inner control law is given by

$$u(t) = \widehat{M}_{qq}(w(t) - S_t(s_x, \Lambda_1, \Lambda_2)), \quad (32)$$

where $\widehat{M}_{qq} = M_{qq}(x_1, \widehat{\Pi}_g, \widehat{\Pi}_d)$. Then, control laws (30) and (32) ensure finite-time exact convergence of the sliding variables s_x and s_y as defined in (29) and (31). Furthermore, the quaternion and angular velocity errors e_c , e_ω are asymptotically stable under the dynamics of $s_y = 0$.

Proof: Using (27) and the torque control assumption, the dynamics of the sliding variable s_x is

$$\dot{s}_x = \dot{x}_2 - w(t) = M_{qq}^{-1} u(t) + x_3 - w(t). \quad (33)$$

Substituting the control law (32) into (33), it becomes

$$\dot{s}_x = -(\mathbf{I}_3 - M_{qq}^{-1} \Delta M_{qq}) S_t(s_x, \Lambda_1, \Lambda_2) + x_3 \quad (34)$$

where $\Delta M_{qq} = M_{qq} - \widehat{M}_{qq}$. Using (19), $\Delta M_{qq} S_t = Y_q^* \widehat{\Pi}_d + \Delta Y_q^* \widehat{\Pi}_d$, with $\Delta Y_q^* = Y_q^* - \widehat{Y}_q^*$, where $Y_q^* = Y_q(x_1, 0, S_t(s_x, \Lambda_1, \Lambda_2), 0, 0, 0, 0, \widehat{\Pi}_g)$ and $\widehat{Y}_q^* = Y_q(x_1, 0, S_t(s_x, \Lambda_1, \Lambda_2), 0, 0, 0, 0, \widehat{\Pi}_g)$. Then, it is possible to rewrite (34) as

$$\begin{aligned} \dot{s}_x &= -\Lambda_1 [s_x]^{1/2} + w_x, \\ \dot{w}_x &= -\Lambda_2 [s_x]^0 + d_x, \end{aligned} \quad (35)$$

where $d_x = \nabla(M_{qq}^{-1} Y_q^*) \widehat{\Pi}_d + \nabla(M_{qq}^{-1} \Delta Y_q^*) \widehat{\Pi}_d + \dot{x}_3$ is clearly dependent on the base motion and on the errors on the geometric and dynamic parameters. Here, the operator ∇ denotes time differentiation.

Note that (35) is STA, which is finite-time stable for bounded disturbances. It is evident that, if the nominal parameters are known, system (34) is only perturbed by $d_x \approx \dot{x}_3$. Due to Assumptions (ii) and (iii), the following inequalities hold:

$$\left\| \nabla(M_{qq}^{-1} Y_q^*) \widehat{\Pi}_d \right\| < L_{x_1}, \quad (36)$$

$$\left\| \nabla(M_{qq}^{-1} \Delta Y_q^*) \widehat{\Pi}_d \right\| < L_{x_2}, \quad (37)$$

$$\|\dot{x}_3\| < L_{x_3}. \quad (38)$$

Then, $\|d_x\| < L_{x_1} + L_{x_2} + L_{x_3}$, and according to (Moreno and Osorio, 2012), it is possible to chose Λ_1 and Λ_2 so that (35) achieves SOSM in finite-time. It means that after a finite time $T_1 > 0$, $s_x = \dot{s}_x = 0$ and due to (33), $\dot{x}_2 = w(t) \forall t > T_1$, even in the presence of the bounded disturbance d_x .

Next, using (28), (21) and (22), the dynamics of the outer sliding variable (29) is given by

$$\dot{s}_y = \dot{y}_{2_d} - J_{0c}^c(x_1) \dot{x}_2 - y_3 + K_c \psi, \quad (39)$$

where $\psi(y_1, y_2, r_{cd}) = y_{11} \dot{y}_{12_d} - 0.5 y_{12}^T y_2 y_{12_d} - \dot{y}_{11_d} y_{12} - \widehat{y}_{12_d} y_{12} - 0.5 y_{11_d} (y_{11} \mathbf{I}_3 - \widehat{y}_{12}) y_2 - 0.5 \widehat{y}_{12_d} (y_{11} \mathbf{I}_3 - \widehat{y}_{12}) y_2$, with $\dot{y}_{1_d} = \mathbf{h}_-(y_1) y_{2_d}$.

Since $\dot{x}_2 = \dot{s}_x + w(t)$, substituting (30) into (39) and using Assumption (i) yields

$$\begin{aligned} \dot{s}_y &= -\Lambda_3 [s_y]^{1/2} + w_y, \\ \dot{w}_y &= -\Lambda_4 [s_y]^0 + d_y, \end{aligned} \quad (40)$$

where $d_y = -\dot{y}_3 - \nabla(J_{0c}^c \dot{s}_x) - \nabla(W_\omega^*) \widehat{\Pi}_g$, with $W_\omega^* = W_\omega(x_1, w(t), 0)$, according to (17). Again, due to Assumptions (ii) and (iii):

$$\|\nabla(J_{0c}^c \dot{s}_x)\| < L_{y_1}, \quad (41)$$

$$\left\| \nabla(W_\omega^*) \widehat{\Pi}_g \right\| < L_{y_2}, \quad (42)$$

$$\|\dot{y}_3\| < L_{y_3}. \quad (43)$$

Note that (41) is true because \dot{s}_x is bounded, but constant L_{y_1} clearly depends on the initial conditions of (27). Also, in (42), $\nabla(W_\omega^*)$ depends on x_1 , x_2 , $w(t)$ and $\dot{w}(t)$, which are also bounded. Then, $\|d_y\| < L_{y_1} + L_{y_2} + L_{y_3}$, again guaranteeing finite-time stabilization of (40) after a time $T_2 > 0$. It means that for all $t \geq T_2$, the system is sliding and therefore, it follows the nonlinear dynamics of the sliding variable (29), which is asymptotically stable (Siciliano et al., 2009). Therefore, the quaternion errors (21) and (22) tend to zero asymptotically after a time $\max(T_1, T_2)$. \square

4.2 Super-Twisting Control with HOSM Observer

If state $x_2 \in \mathbb{R}^3$ is not available, an observer could be used to estimate the joint velocity state $x_2(t)$ using the measurements of $x_1(t)$. Because of its desired characteristics such as finite-time exact convergence, sliding mode observers could be used for this purpose, such as the *super-twisting* observer (STO) (Moreno and Osorio, 2012). However, according to (Chalanga et al., 2016), it is not possible to achieve *second order sliding* ($s = \dot{s} = 0$) using *continuous* control when STC is implemented based on ST observers. A proposed solution is to use STC with HOSM-based observers to achieve continuous control.

Theorem 2 (Cascade STC with Output Feedback) Let (27) and (28) be the system dynamic and kinematic models.

Defining the estimation error $e_{x_1} = x_1 - \widehat{x}_1$, the HOSM observer for x_2 is the third-order system

$$\begin{aligned} \dot{\widehat{x}}_1 &= K_1 [e_{x_1}]^{2/3} + \widehat{x}_2, \\ \dot{\widehat{x}}_2 &= K_2 [e_{x_1}]^{1/3} + \widehat{x}_3 + \widehat{M}_{qq}^{-1} u, \\ \dot{\widehat{x}}_3 &= K_3 [e_{x_1}]^0, \end{aligned} \quad (44)$$

where K_1 , K_2 and K_3 are positive-definite matrices. The outer sliding variable and control law

are defined in the same way as (29) and (30). The modified inner sliding variable is

$$\widehat{s}_x = \widehat{x}_2 - \int_0^t w(\tau) d\tau, \quad (45)$$

and the corresponding inner control law is

$$u(t) = \widehat{M}_{qq} \left(w(t) - K_2 [e_{x_1}]^{1/3} - S_t(\widehat{s}_x, \Lambda_1, \Lambda_2) \right). \quad (46)$$

Then, under the same assumptions of Theorem 1, control laws (46) and (30) with observer (44) ensure finite-time exact convergence of the sliding variables s_x and s_y as defined in (45) and (29), and of the estimation errors e_{x_1} , $e_{x_2} = x_2 - \widehat{x}_2$ and $e_{x_3} = x_3 - \widehat{x}_3$. Furthermore, the quaternion and angular velocity errors e_c , e_ω are asymptotically stable under the dynamics of $s_y = 0$.

Proof: Using (27) and (44), the dynamics of the estimation errors is

$$\begin{aligned} \dot{e}_{x_1} &= -K_1 [e_{x_1}]^{2/3} + e_{x_2}, \\ \dot{e}_{x_2} &= -K_2 [e_{x_1}]^{1/3} + e_{x_3} + (M_{qq}^{-1} - \widehat{M}_{qq}^{-1})u, \\ \dot{e}_{x_3} &= -K_3 [e_{x_1}]^0 + \dot{x}_3. \end{aligned} \quad (47)$$

By using transformation $e_{x_4} = e_{x_3} + (M_{qq}^{-1} - \widehat{M}_{qq}^{-1})u$, it is possible to rewrite (47) as

$$\begin{aligned} \dot{e}_{x_1} &= -K_1 [e_{x_1}]^{2/3} + e_{x_2}, \\ \dot{e}_{x_2} &= -K_2 [e_{x_1}]^{1/3} + e_{x_4}, \\ \dot{e}_{x_4} &= -K_3 [e_{x_1}]^0 + d_e, \end{aligned} \quad (48)$$

where $d_e = \dot{x}_3 + (M_{qq}^{-1} - \widehat{M}_{qq}^{-1})\dot{u} + \nabla(M_{qq}^{-1} - \widehat{M}_{qq}^{-1})u$. Due to Assumption (ii) and (46), two constants $L_{e_1}, L_{e_2} > 0$ exist, such that:

$$\left\| (M_{qq}^{-1} - \widehat{M}_{qq}^{-1})\dot{u} \right\| < L_{e_1}, \quad (49)$$

$$\left\| \nabla(M_{qq}^{-1} - \widehat{M}_{qq}^{-1})u \right\| < L_{e_2}. \quad (50)$$

Also, by Assumption (iii), $\|\dot{x}_3\| < L_{x_3}$ also holds. Then, $\|d_e\| < L_{e_1} + L_{e_2} + L_{x_3}$, and therefore the disturbance d_e is norm-bounded. According to (Moreno, 2012), it is possible to chose K_1, K_2 and K_3 so that the states on (48) are finite-time stable.

Remark 6 Since $M_{qq}^{-1} - \widehat{M}_{qq}^{-1} \neq 0$ due to parametric uncertainty, the estimation error e_{x_3} is expected to be norm-bounded only. Therefore, $x_3 = \widehat{x}_3 + \beta(\Pi)$, where $\beta(\Pi)$ is a small residue dependent on the parametric uncertainty.

The dynamics of the modified sliding variable is given by

$$\dot{\widehat{s}}_x = K_2 [e_{x_1}]^{1/3} + \widehat{x}_3 + \widehat{M}_{qq}^{-1}u(t) - w(t). \quad (51)$$

Using the continuous control law (46), yields:

$$\begin{aligned} \dot{\widehat{s}}_x &= -\Lambda_1 [\widehat{s}_x]^{1/2} + \widehat{w}_x, \\ \dot{\widehat{w}}_x &= -\Lambda_2 [\widehat{s}_x]^0 + K_3 [e_{x_1}]^0. \end{aligned} \quad (52)$$

Since the disturbance $K_3 [e_{x_1}]^0$ is obviously norm-bounded, the STA (52) is finite-time stable. Therefore, after a finite time $\bar{T}_1 > 0$, $\dot{x}_2 = w(t)$.

To prove the stability of the outer controller, a similar procedure is performed. Since $\dot{x}_2 = \widehat{s}_x + \dot{e}_{x_2} + w(t)$, substituting (30) into (39) and using Assumption (i) yields

$$\begin{aligned} \dot{s}_y &= -\Lambda_3 [s_y]^{1/2} + w_y, \\ \dot{w}_y &= -\Lambda_4 [s_y]^0 + \bar{d}_y, \end{aligned} \quad (53)$$

with $\bar{d}_y = -\dot{y}_3 - \nabla(J_{0c}^c \dot{\widehat{s}}_x) + \nabla(J_{0c}^c \dot{e}_{x_2}) - \nabla(W_\omega^*)\widetilde{\Pi}_g$. Again, due to Assumptions (ii) and (iii), (48) and (52), two positive constants $\bar{L}_{y_1}, \bar{L}_{y_2}$ exist, such that

$$\left\| \nabla(J_{0c}^c \dot{\widehat{s}}_x) \right\| < \bar{L}_{y_1}, \quad (54)$$

$$\left\| \nabla(J_{0c}^c \dot{e}_{x_2}) \right\| < \bar{L}_{y_2}. \quad (55)$$

Then, $\|\bar{d}_y\| < \bar{L}_{y_1} + \bar{L}_{y_2} + L_{y_2} + L_{y_3}$, again guaranteeing finite-time stabilization of (53) after a time $\bar{T}_2 > 0$. Therefore, the quaternion errors (21) and (22) tend to zero asymptotically after a time $\max(\bar{T}_1, \bar{T}_2)$. \square

5 Simulation Results

MATLAB Simulink[®] models were implemented for the simulation of the dynamic model of a 3-DOF ISP installed on a vessel and the proposed control strategies.

Remark 7 The presented control methods can be applied to any kind of vehicle or moving base where the ISP is installed, since the quaternion formalism does not suffer from representation singularities and the base dynamics (velocities and accelerations) only affect the overall magnitude of the gains.

Joint friction torques were simulated as the sum of Stribeck, Coulomb and viscous friction components, and a saturation of $\pm 12.2 Nm$ in each joint motor was considered. The joint encoders and the INS were modeled considering hardware effects such as resolution, bias and noise, and the base motion data were obtained from the simulation of a vessel subject to Jonswap spectrum waves with 200 harmonics, 3m height, 10s time period, and acting on the longitudinal axis of the vessel.

Table 1 contains the kinematic and dynamic parameters used in the simulations. The real joint axis are considered as $h_1^0 = z_0$, $h_2^1 = y_0$ and $h_3^2 = x_0$. Also, we have $p_{3c}^3 = [0.555 \ 0 \ 0.014]^\top$, and the inertia tensor represented in \mathbf{E}_i can be computed

Table 1: Kinematic and dynamic model parameters, in SI units.

Parameter	$i = 1$			$i = 2$			$i = 3$		
	x	y	z	x	y	z	x	y	z
p_{ii}^i	0.006	0.023	0.326	-0.094	0.006	0.059	0.336	0.006	-0.023
$p_{i-1,i}^{i-1}$	0.3	0	0	0	0	0.436	-0.254	0	0
I_i^i	2.42	0.58	1.93	1.12	0.92	0.88	0.54	0.93	0.86
m_i	18.9			21			26.5		

from the *Huygens-Steiner theorem* as $I_i^i = I_i^{\bar{i}} - m_i (\hat{p}_{i\bar{i}}^i)^2$.

The values for the nominal parameters used in control were set as the real values in Table 1 with a percentage of error. The gains for both state and output feedback controllers were set as $\Lambda_1 = \Lambda_2 = 5 \mathbf{I}_3$, $\Lambda_3 = \Lambda_4 = 10 \mathbf{I}_3$, and the HOSMO gains were chosen as $K_1 = K_2 = K_3 = 10$. These values are sufficient to overcome the magnitude of the disturbances and small enough to avoid chattering effects.

The target point inertial reference p_t is a circular pattern on the XY plane, expressed by

$$p_t = \begin{bmatrix} p_{t_x} + R(\sin(\omega t) + \sin(4\omega t)) \\ p_{t_y} + R(\cos(\omega t) + \cos(4\omega t)) \\ p_{t_z} \end{bmatrix}, \quad (56)$$

with $p_{t_x} = 0$, $p_{t_y} = 100$, radius $R = 25$ and angular frequency $\omega = 0.0628 \text{ rad/s}$. The references y_{1d} , y_{2d} and \dot{y}_{2d} were obtained from (23), (24) and (25), respectively.

5.1 Full State Feedback STC

Figure 1 shows the transient and steady-state response of the state feedback STC in terms of RPY errors for the case of 50% of parametric error and 5° degrees of axis misalignment in the computation of the Jacobian matrix. Both stabilization

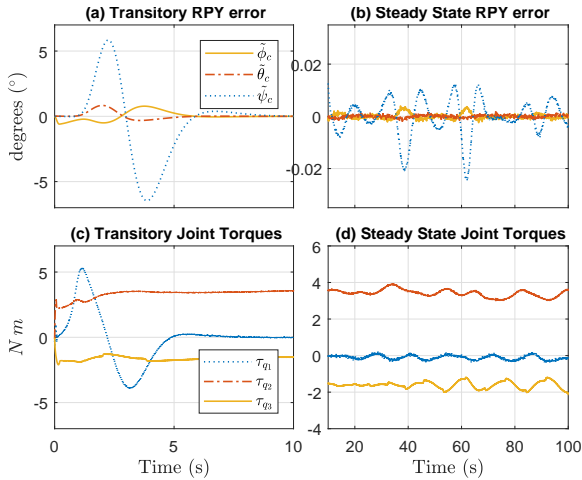


Figure 1: Response for state feedback STC controller with 50% of parametric error and 5° degrees of axis misalignment.

and tracking controllers achieve SOSM in less than 2 s, with sliding accuracy on s_x and s_y approximately equal to 10^{-5} . The RPY jitter converges to a small region of 0.03° in approximately 10 s due to the chosen dynamics for the outer sliding surface.

5.2 Output Feedback STC + HOSMO

Figure 2 shows the transient and steady-state response of the of the output feedback STC, in the same conditions as before. The transient and per-

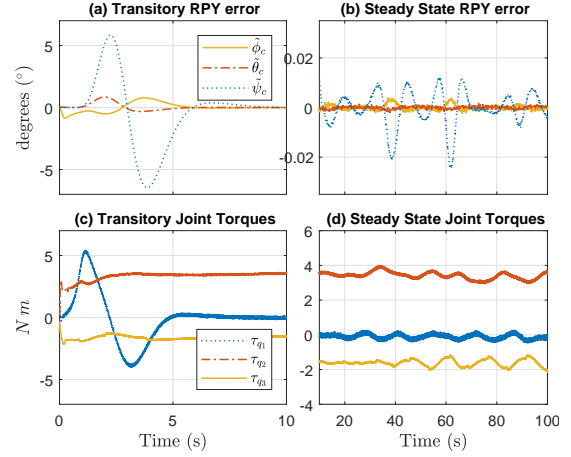


Figure 2: Response for output feedback STC controller with 50% of parametric error and 5° degrees of axis misalignment.

formance remains practically the same, with a very small increase in the RPY jitter and in the control chattering. This is due to the presence of the term dependent multiplying K_2 in (46).

Figure 3 shows the HOSMO estimation errors of the output feedback STC scheme. Note

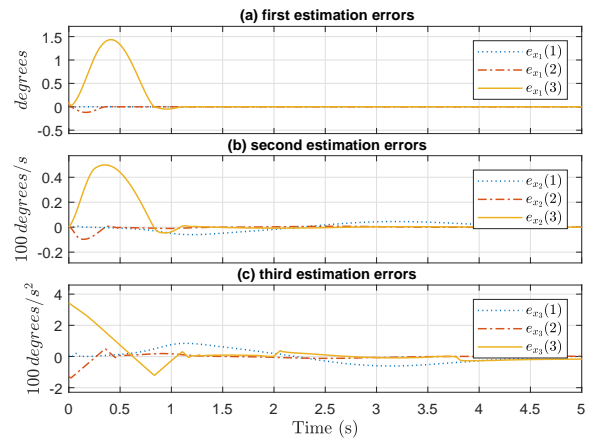


Figure 3: HOSMO estimation errors for output feedback STC controller with 50% of parametric error.

that finite-time convergence is achieved in approximately 1.2 s, even in the presence of sensor noise and 50% of parametric error in \widehat{M}_{qq} used in (44).

6 Conclusion

Although both control algorithms use the ISP mass matrix and its geometrical Jacobian, the obtained tracking accuracy is much better than with P-PI or computed torque control (Reis et al., 2018), even in the presence of strong parametric uncertainty and sensor noise. Besides, considering the amplitude and frequency of the control chattering, it is reasonable to conclude that this scheme could be implemented in a real system.

In general, the performance of the output feedback STC is very close to the full state feedback STC, but with the clear advantage of avoiding taking joint velocity measurements.

References

- Abdo, M. M., Vali, A. R., Toloie, A. R. and Arvan, M. R. (2014). Stabilization loop of a two axes gimbal system using self-tuning pid type fuzzy controller, *ISA Transactions* **53**(2): 591 – 602.
- Abdo, M., Vali, A. R., Toloie, A. and Arvan, M. R. (2013). Research on the cross-coupling of a two axes gimbal system with dynamic unbalance, *International Journal of Advanced Robotic Systems* **10**.
- Chalanga, A., Kamal, S., Fridman, L. M., Bandyopadhyay, B. and Moreno, J. A. (2016). Implementation of super-twisting control: Super-twisting and higher order sliding-mode observer-based approaches, *IEEE Transactions on Industrial Electronics* **63**(6): 3677–3685.
- Debruin, J. (2008). Control systems for mobile satcom antennas, *Control Systems, IEEE* **28**(1): 86–101.
- Feng, Y., Yu, X. and Man, Z. (2002). Non-singular terminal sliding mode control of rigid manipulators, *Automatica* **38**(12): 2159 – 2167.
- From, P. J., Gravdahl, J. T. and Pettersen, K. Y. (2014). *Vehicle-manipulator systems*, Springer.
- Hilkert, J. M. (2008). Inertially stabilized platform technology: Concepts and principles, *IEEE Control Systems Magazine* **28**(1): 26–46.
- Hurák, Z. and Řezáč, M. (2009). Combined line-of-sight inertial stabilization and visual tracking: application to an airborne camera platform, *Proceedings of the IEEE Conference on Decision and Control.*, pp. 8458–8463.
- Kazemy, A., Hosseini, S. A. and Farrokhi, M. (2007). Target-based line-of-sight stabilization in periscopes, *Mediterranean Conference on Control and Automation* .
- Kennedy, P. J. and Kennedy, R. (2014). *Stabilizing the Line of Sight*.
- Kennedy, P. J. and Kennedy, R. L. (2003). Direct versus indirect line of sight (LOS) stabilization, *IEEE Transactions on Control Systems Technology* **11**(1): 3–15.
- Königseder, F., Kemmetmüller, W. and Kugi, A. (2017). Attitude control strategy for a camera stabilization platform, *Mechatronics* **46**: 60–69.
- Levant, A. (2003). Higher-order sliding modes, differentiation and output-feedback control, *International Journal of Control* **76**(9-10): 924–941.
- Mao, J., Yang, J., Li, S. and Li, Q. (2017). Output feedback stabilization of inertial stabilized platform with unmatched disturbances using sliding mode approach, **50**: 5149–5154.
- Masten, M. K. (2008). Inertially stabilized platforms for optical imaging systems, *IEEE Control Systems Magazine* **28**(1): 47–64.
- Moreno, J. A. (2012). Lyapunov function for levant’s second order differentiator, *2012 IEEE 51st IEEE Conference on Decision and Control (CDC)*, pp. 6448–6453.
- Moreno, J. A. and Osorio, M. (2012). Strict lyapunov functions for the super-twisting algorithm, *IEEE Transactions on Automatic Control* **57**(4): 1035–1040.
- Reis, M., Carvalho, G. P. S., Neves, A. F. and Peixoto, A. J. (2018). Dynamic model and line of sight control of a 3-dof inertial stabilization platform, *Proceedings of the IEEE American Control Conference*.
- Siciliano, B., Sciavicco, L. and Villani, L. (2009). *Robotics : Modelling, Planning and Control*, Advanced Textbooks in Control and Signal Processing, Springer, London. 013-81159.
- Skjelten, H., Gutvik, C. and Solberg, L. (2011). Ship based oil spill monitoring: A new integrated system for thickness evaluation and operational overview, *International Oil Spill Conference Proceedings (IOSC)*, Vol. 2011, American Petroleum Institute.
- Vilhena Adorno, B. (2017). Robot Kinematic Modeling and Control Based on Dual Quaternion Algebra — Part I: Fundamentals. working paper or preprint.